Quantum Dot–Carrier Peptide Conjugates Suitable for Imaging and Delivery Applications

ARTICLE *in* BIOCONJUGATE CHEMISTRY · DECEMBER 2008

Impact Factor: 4.51 · DOI: 10.1021/bc800172q · Source: PubMed

Quantum Dot−Carrier Peptide Conjugates Suitable for Imaging and Delivery Applications

Cornelia Walther, Karolin Meyer, Robert Rennert, and Ines Neundorf*

Institute of Biochemistry, Faculty of Biosciences, Pharmacy and Psychology, University of Leipzig, Brüderstr. 34, 04103 Leipzig.
Received April 25, 2008; Revised Manuscript Received September 5, 2008

We developed multifunctional fluorescent nanoparticles suitable for the nonviral delivery of negatively charged molecules like RNA. Therefore, we incorporated the recently developed branched hCT-derived carrier peptide hCT(18−32)-k7 on the surface of luminescent quantum dots (QDs). Besides detailed characterization of our QD−peptide conjugates concerning stability, toxicity, and uptake mechanism. we used them for efficient RNA delivery into different cell lines. The results of our studies indicate the involvement of more than one endocytotic uptake pathway in the internalization process. Furthermore, we could show that the QD−peptide bioconjugates exhibit no effect on cell viability and possess high stability inside living cells. The efficacy of our newly designed constructs for oligonucleotide drug delivery is highlighted by the successful intracellular transport of Cy-3 labeled RNA. Moreover, by using the chemotherapeutic chloroquine the efficient release of the assemblies out of endosomes was demonstrated. These results prove that our multifunctional platforms are versatile tools for diagnostic and therapeutic imaging purposes applicable for biologically active siRNA or aptamer sequences.

INTRODUCTION

During the past decades, a large amount of potential drug candidates and future drug targets have been developed. Our main focus should now rest on the understanding and investigation of the biological action and processes these compounds exert and cause. For this reason, it is not only important to figure out how a probe enters a cell but also to follow its fate within the cell interior. Recently, a series of multifunctional nanoparticles has been developed that can be used in biomedical and pharmaceutical applications for diagnosis and therapy. Thereby, these probes can not only serve as vehicles for the delivery of therapeutic agents to their targets, but they can also act as tools for imaging. The latter can be realized by the use of luminescent semiconductor nanocrystals, also known as quantum dots (QDs). Due to unique spectroscopic properties, this new class of materials has attracted much attention (*1, 2*). Quantum dots have narrow, size-tunable emission spectra and possess a high quantum yield. They are excitable within a broad wavelength range and are exceptionally resistant to photobleaching and chemical degradation. All these advantages make them superior to conventionally used fluorophor systems like small organic dyes or fluorescent proteins. For this reason, they are widely applied as an alternative in many fluorescent-based (cell-) assays preferably when performing long-term and multicolor labeling experiments (*3*). However, certain requirements should be fulfilled by these particles: they should not exhibit any cytotoxicity, and they should be attached to a targeting moiety allowing them not only to penetrate the cell membrane but also to reach their target site within the cell interior.

Coating QDs with peptides is one approach that has become more and more accepted. For instance, attachment of cell-penetrating peptides (CPP) (*4, 5*), such as polyarginine and TAT-derived peptides, to the QD surface has allowed translocating QDs into cells (*6, 7*). Recently, CPP have become widely used vectors for the cellular delivery of molecules in basic and applied biomedical research. With their help, it is possible to introduce membrane-impermeable substances like peptide nucleic acids (PNA) (*8*), proteins (*9*), oligonucleotides (*10*), or nanoparticels (*11, 12*) into mammalian cells. There is a growing attraction in using CPP for drug delivery because many pharmacologically interesting molecules have often only poor bioavailability. Additionally, the attachment of the bioactive compound is easily achieved by covalent coupling or via complexation strategies. Cell-penetrating properties of the human hormone calcitonin (hCT) have been described recently. Human calcitonin, a 32 amino acid long peptide amide, is physiologically secreted by the thyroid gland and involved in the regulation of the calcium metabolism. Owing to a high permeability through the nasal epithelium, it is applied as an intranasal therapeutic (*13*). Structure−activity studies revealed that the truncated sequence hCT(9−32) can translocate through cell membranes, although the calcitonin receptor activating N-terminus (aa 1−8) of hCT is lacking (*14, 15*). By using hCT(9−32), efficient transport of different cargoes into cells like the antiproliferative drug daunorubicin, fluorophors, or even large proteins has been achieved (*16, 17*). Until now, several different hCT-derived carrier peptides have been developed and successfully used in internalization studies (*18, 19*). Moreover, we previously reported on branched hCT-derived analogues that very effectively transfected several cell lines, as well as primary cells, with plasmid DNA encoding the protein EGFP (*20, 21*). This branched design successfully combined the cell-penetrating properties of the hCT moiety with a positively charged side chain suitable for complexation of negatively charged molecules like oligonucleotides. However, so far little is known about the uptake mechanism of hCT-derived CPP. From several studies, it is known that the uptake is mediated by endocytosis. Recently, Foerg et al. postulated a lipid raft dependent pathway for hCT(9−32) and its branched derivative hCT(9−32)-br into cells (*22*). For future applications, a further careful analysis of the uptake mechanism is crucial. In particular, the correlation between attached cargoes and the entry pathway should be

* Corresponding author. Dr. Ines Neundorf, Faculty of Biosciences, Pharmacy and Psychology, Institute of Biochemistry, Brüderstr. 34, D-04103 Leipzig, Phone: +49 (0) 341 97 36 832, Fax: +49 (0) 341 97 36 909, E-mail: neundorf@uni-leipzig.de.

10.1021/bc800172q CCC: $40.75
Published on Web 11/08/2008

investigated carefully. Results from these studies should help to design best-fitted hCT-derivatives.

The focus of this work was the design and characterization of a QD−peptide-based delivery system suitable for imaging and delivery purposes. Therefore, we covalently coupled a branched hCT-derived peptide to QD nanoparticles of different colors. For the first time, we present the successful delivery of nanoparticles with our hCT-derived CPP. Furthermore, the newly generated constructs were investigated concerning cellular toxicity, stability, and uptake mechanism. Additionally, we focused on the cellular transport of potent oligonucleotide drugs and chose Cy-3-labeled RNA for tracking the fate of the cargo in the cytoplasm. By using fluorescence microscopy, we could demonstrate an effective uptake of these QD−peptide−RNA conjugates and that the complex between the RNA and the QD−peptide conjugate is quite stable. Moreover, by the addition of chloroquine, a substance that assists the release out of endosomes, the assemblies of RNA and QD−peptide conjugates diffused in the cytoplasm.

EXPERIMENTAL PROCEDURES

Materials. Piperidine, thioanisole, ethanedithiole, trifluoroacetic acid (TFA) (HPLC grade), tris(2-carboxyethyl)phosphine (TCEP), Trypan blue, Hoechst 33342, and 5(6)-carboxyfluorescein (CF) were purchased from Fluka (Buchs, Switzerland). *N,N*-Diisopropylethylamine (DIEA), *O*-(7-azabenzotriazol-1-yl)-1,1,3,3-tetramethyluronium hexafluorophosphate (HATU), thiocresol, ethylenediaminetetraacetic acid (EDTA), methyl-β-cyclodextrin, wortmannin, chlorpromazine, 5-(*N*-ethyl-*N*-isopropyl)amiloride (EIPA), nystatin, and sulfosuccinimidyl 4-(*N*-maleimidomethyl)cyclohexane-1-carboxylate (sulfo-SMCC) were obtained from Sigma-Aldrich (Steinheim, Germany). Quantum Dots (T2-MP-EviTags) from Evident Technologies (New York, USA), diethyl ether from Merck (Darmstadt, Germany), and acetonitrile (ACN) were purchased from VWR Prolabo (Darmstadt, Germany). 4-(2′,4′-Dimethoxyphenyl-Fmoc-aminoethyl)-phenoxy resin (Rink amide) and N^{α}-Fmoc-protected amino acids were purchased from NovaBiochem (Läufelingen, Switzerland) and Iris Biotech (Marktredwitz, Germany). *N,N*′-Diisopropylcarbodiimide (DIC), *N*-hydroxybenzotzriazole (HOBt), and trifluoroacetic acid (TFA) (peptide grade) were obtained from Iris Biotech (Marktredwitz, Germany). *N,N*′-Dimethylformamide (DMF) and dichloromethane (DCM) were purchased from Biosolve (Valkenswaard, The Netherlands).

The following side chain protecting groups were chosen: trityl (Trt) for Cys and His; 2,2,4,6,7-pentamethyldihydrobenzofurane-5-sulfonyl (Pbf) for Arg; *tert*-butyl (tBu) for Thr and Glu; *tert*-butyloxylcarbonyl (Boc) or 1-(4,4-dimethyl-2,6-dioxocyclohex-1-ylidene)ethyl (Dde) according to the synthesis strategy.

For cell culture and colocalization studies, the following media, supplements, and substances were used: RPMI 1640 (with L-glutamine), Dulbecco's modified Eagle's medium (DMEM), trypsin/EDTA (1 × concentrate, 1:250 in PBS, trypsin 0.5 mg/mL, EDTA 0.22 mg/mL, pH 7−7.5), Dulbecco's phosphate buffered saline (PBS, pH 7.4), and fetal calf serum (FCS) were purchased from PAA Laboratories (Pasching, Austria), OptiMEM and Hank's balanced salt solution (HBSS) from Gibco/Invitrogen (Auckland, NZ). Transferrin from human serum as Texas Red or Alexa Fluor 488 conjugate and cholera toxin subunit B (recombinant) Alexa Fluor 488 or 647 conjugate were from Molecular Probes (Eugene, Oregon, USA). Cell culture flasks (75 cm^2) and 24-well plates were obtained from TPP (Trasadingen, Switzerland). 8-well chamber slides for microscopy were from ibidi (Munich, Germany). Human embryonic kidney (HEK 293) and human cervix carcinoma (HeLa) cell lines were obtained from the American type Culture Collection (ATCC).

Peptide Synthesis and Purification. Synthesis of the hCT derivatives was performed by automated multiple solid-phase peptide synthesis (SPPS) (Syro, MultiSynTech, Bochum, Germany) using orthogonal Fmoc/^{t}Bu strategy as described previously (*23*). All peptides were synthesized as C-terminal amides by using the Rink amide resin (30 mg, resin loading 0.45 mmol g^{-1}).

At first the sequence, hCT(19−32) was synthesized automatically. Then, (Dde)-Lys(Fmoc)-OH was introduced manually and elongated via the side chain of Lys (*18*) to obtain the branched peptides. Therefore, double-coupling reactions were carried out (1 h each) using 3-fold excess of amino acid, HATU, and DIEA. Afterward, the fragment was elongated automatically and (Dde)-hCT(18−32)-k7 was obtained, whereas the N-terminus of the side chain k7 was protected with Boc. After cleavage of the Dde protecting group with 2% hydrazine in DMF (v/v; 10 × 10 min at room temperature), the peptide was either modified with (5,6)-carboxyfluorescein (CF) or cysteine in order to obtain CF-hCT(18−32)-k7 or [C^{17}]-hCT(18−32)-k7, respectively. CF-coupling was performed for 2 h using a 1.5-fold excess of CF, HATU, and DIEA in DMF. Introduction of cysteine was performed as described above for (Dde)-Lys(Fmoc)-OH. For synthesis of a double-labeled conjugate, CF-labeling of the side chain occurred as described above. Subsequently, the hydroxyl groups of CF were protected with trityl by using 4 equiv of trityl chloride and DIEA in DCM for 16 h. Then, cysteine at position 17 was introduced after cleavage of the Dde protecting group.

Finally, the peptides were cleaved from the resins within 3 h at room temperature. Peptides without Cys were treated with TFA/thioanisol/thiocresol (90:5:5 v/v) and peptides containing Cys were treated with TFA/thianisol/ethanedithiol (90:7:3 v/v). Then, the peptides were precipitated from ice−cold diethyl ether, collected by centrifugation, lyophilized from water/*tert*-butyl alcohol (3:1 v/v), and analyzed by analytical RP-HPLC on a Vydac RP18-column (4.6 × 250 mm; 5 μm/300 Å) using linear gradients of 10−60% B in A (A = 0.1% TFA in water; B = 0.08% TFA in ACN) over 30 min and a flow rate of 0.6 mL min^{-1}. Purification of the peptides was achieved by preparative HPLC on a RP18 column (Waters, 5 μm, 25 × 300 mm) by using a linear gradient of 10−40% B in A over 50 min and a flow rate of 15 mL min^{-1}. Identification was performed by MALDI-TOF mass spectrometry (Voyager RP, Perseptive Biosystems), and purity was confirmed again by analytical RP-HPLC as described before.

The following peptides were synthesized: CF-hCT(18−32)-k7, [C^{17}]-hCT(18−32)-k7, and [C^{17}]-hCT(18−32)-k7(CF). Sequences and analytical data are shown in Table 1.

Preparation of QD−Peptide Conjugates. To obtain QD-[C^{17}]-hCT(18−32)-k7 conjugates, amine-functionalized quantum dots (QD; purchased from EvidentTech) were at first activated by adding approximately 1 mg of sulfo-SMCC to 200 μL of amine quantum dots (QD_{514}: n = 2.3 nmol) in 200 μL of 50 mM sodium phosphate pH 7.4. After shaking at room temperature for 60 min, the excess of the cross-linker was removed using a PD-10 desalting column equilibrated with conjugation buffer (1 mM EDTA, 0.1 M phosphate, 0.15 M NaCl, pH 7.2). Fractions containing the QD were collected, identified by tracking the fluorescence (Horiba Jobin Yvon Fluorolog-3), and combined. Coupling of the peptide was performed by first incubating the peptide with TCEP to obtain free sulfhydryl groups. Then, [C^{17}]-hCT(18−32)-k7 was mixed with the maleimide-activated QD in conjugation buffer (1 mM EDTA, 0.1 M phosphate, 0.15 M NaCl, pH 7.2) and incubated at 4 °C overnight. Afterward, the solution was concentrated using an Amicon filter device (MWCO 10 000). The conjugate was then purified by size exclusion chromatography with a

Table 1. Amino Acid Sequences, Molecular Masses and Retention Times of the Synthesized hCT-Derivatives

Peptide	Sequence	MW [Da] calc.	MW [Da] exp.	t_{ret} [min]
CF-hCT(18-32)-k7[a]	**CF**-KFHTFPQTAIGVGAP-NH_2 KKRKAPKKKRKFA⌟	3523.2	3524.4	15.3
[C^{17}]-hCT(18-32)-k7	C^{17}KFHTFPQTAIGVGAP-NH_2 KKRKAPKKKRKFA⌟	3268.0	3268.7	14.3
[C^{17}]-hCT(18-32)-k7(**CF**)	C^{17}KFHTFPQTAIGVGAP-NH_2 **CF**-KKRKAPKKKRKFA⌟	3626.6	3627.8	14.7

[a]CF: 5(6)-carboxyfluorescein.

Superdex200 resin. At least 25−30 fractions were collected. The fluorescence of the fractions was recorded at the QD emission peak wavelength of 514 nm, and the peptide amount in each fraction was measured by Bradford assay. The Bradford readings and the fluorescence values at the QD emission peak wavelength were plotted vs the fraction number to generate elution profiles and to identify the fractions containing QD−peptide conjugate.

The same procedure was used to conjugate [C^{17}]-hCT(18−32)-k7 and [C^{17}]-hCT(18−32)-k7(CF) to QD_{617} (n = 2.4 nmol). QD−peptide conjugates with a QD to peptide ratio of 1:100 up to 1:300 were prepared.

Cell Culture. Cells were grown in 75 cm^2 culture flasks to confluence at 37 °C and 5% CO_2 in a humidified atmosphere (95%). HeLa cells were grown in supplemented RPMI 1640 (with L-glutamine) with 10% heat-inactivated fetal calf serum. HEK 293 cells were cultured in Dulbecco's modified Eagle's medium/Ham's F12 (without L-glutamine) containing 15% heat-inactivated fetal calf serum.

Resazurin-Based Cell Viability Assay. HEK 293 or HeLa cells were seeded in 96-well plates (15 000 and 50 000 cells/well, respectively). To investigate the influence of the inhibitors, peptides, and QD−peptide bioconjugates on the cell viability, we used the fluorimetric resazurin-based cell viability assay as described recently in ref *21*. The peptide or rather the QD−peptide bioconjugate was diluted to appropriate concentrations (0.01−2 μM for the QD−peptide bioconjugate, 100 μM of [C^{17}]-hCT(18−32)-k7 and CF-hCT(18−32)-k7) in standard cell culture medium. For testing the inhibitors, dilutions of wortmannin (200 nM), EIPA (100 μM), chloropromazine (20 μM), nystatin (27 μM), or methyl-β-cyclodextrin (10 mM) in serum free medium were prepared. For each data point, a triplicate of wells was prepared. Cells were incubated for 24 h with the peptide and QD−peptide solutions and for 60 min with the inhibitor solutions, and afterward, the resazurin-based *in vitro* toxicity assay was performed.

Untreated cells were investigated as the negative control, whereas cells incubated with a solution of 70% alcohol for 10 min were used as the positive control. Afterward, a freshly prepared resazurin solution (1:5 v/v in serum-free cell culture medium) was added (1:1 v/v), and the cells were incubated for 2 h under standard growth conditions. The cell viability was finally analyzed fluorimetrically by using a multiwell plate reader (Spectrafluor plus, Tecan, Crailsheim, Germany). The metabolic conversion of resazurin to the reduced resofurin by the living cells was measured at 595 nm (after excitation at 550 nm).

Fluorescence Microscopic Imaging. To characterize the peptide uptake by fluorescence microscopic imaging, living, unfixed cells were investigated. HeLa and HEK 293 cells seeded in 8-well chamber slides (40 000 and 100 000 cells/well, respectively) were incubated with 25 μM CF-hCT(18−32)-k7 for 30 and 60 min. 10 min prior to the end of the peptide incubation, Hoechst 33342 was added to a final concentration of 5 μg/mL for nuclear staining. To monitor the intracellular fate, cells were coincubated with either Alexa Fluor 647 labeled cholera toxine (final concentration of 10 μg/mL) or Texas Red labeled transferrin (final concentration of 50 μg/mL). To distinguish between internalized and cell surface-bound peptides, the remaining extracellular fluorescence was quenched with an acidic Trypan blue buffer (300 μM in glycine buffer, pH 4.5) for 1 min. Subsequently, cells were washed 3 times with PBS, suspended in HBSS (pH 7), and inspected by fluorescence imaging. The peptide uptake was analyzed using a Zeiss Axiovert 200 inverse phase-contrast fluorescence microscope provided with an ApoTome and a 63×/1.4 oil immersion objective.

Additionally, HeLa and HEK 293 cells, seeded in 8 well chamber slides (40 000 and 100 000 cells/well, respectively) were incubated with QD_{617}-[C^{17}]-hCT(18−32)-k7 (0.02 μM QD) for 45 up to 90 min as described above and simultaneously incubated with either cholera toxin Alexa Fluor 488 (10 μg/mL) or transferrin Alexa Fluor 488 (50 μg/mL). Finally, the cells were washed with PBS for several times, diluted in HBSS (pH 7), and imaged.

Flow Cytometry. HeLa and HEK 293 cells were seeded in 24-well plates (100 000 and 250 000 cells/well, respectively) and grown under standard growth conditions. Subconfluent cells were incubated with CF-hCT(18−32)-k7 (20 μM in serum free medium) for 60 min or with QD_{617}-[C^{17}]hCT(18−32)-k7 (0.01 μM QD in serum free medium) for 90 min. Then, cells were incubated with Trypan blue (300 μM in glycine buffer, pH 4.5) for 1 min in order to quench potentially remaining extracellular fluorescence caused by CF. Additionally, cells were washed with PBS (3 × 300 μL). Afterward, the cells were detached by incubation with trypsin/EDTA for 1 min. The catalytic activity of trypsin was stopped by addition of cell culture medium supplemented with 10% FCS (HeLa)/15% FCS (HEK 293). Then, trypsin/EDTA was removed, and the cells were resuspended in PBS and analyzed by a flow cytometer (Partec GmbH, Münster, Germany). At least 10 000 cells per sample were analyzed in order to get reproducible results. The mean fluorescence intensity of peptide-labeled cells was compared with untreated cells as control.

For inhibition of endocytosis pathways, cells were pretreated for 30 min with wortmannin (200 nM), EIPA (100 μM), chloropromazine (20 μM), nystatin (27 μM) or methyl-β-cyclodextrin (10 mM) (all inhibitor dilutions were prepared in serum free medium) prior to incubation with CF- or QD_{617}-

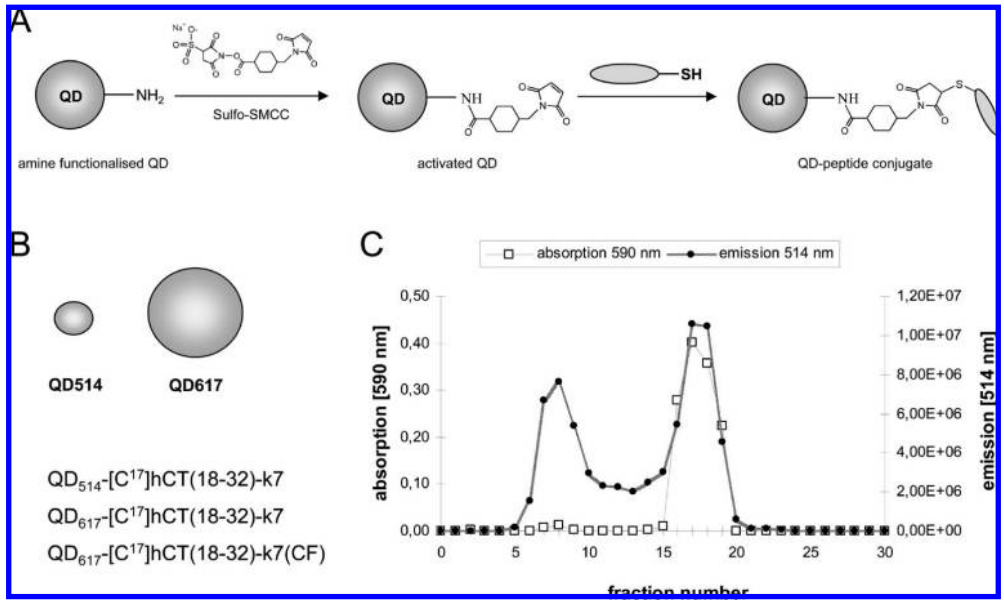

Figure 1. Synthesis of QD−peptide assemblies. (A) Amine-functionalized QDs were activated with sulfo-SMCC, subsequently followed by reaction with the thiol group of the peptide. (B) Two different QDs were used for bioconjugate generation. The double-labeled conjugate was created by coupling the CF-labeled peptide to QD_{617}. (C) Fractions collected by a Superdex200 column were measured by Bradford assay (absorption) and fluorescence spectroscopy (emission). QD−peptide fractions are represented by peaks with overlapping fluorescence and absorption spectra.

labeled hCT derivatives. All experiments were performed twice or triply in duplicate or triplicate.

The flow cytometric data were evaluated by using the software *FlowMax 3.0* (Partec).

Stability of QD-hCT-Peptide Conjugates. To determine the stability of the newly synthesized QD-hCT-peptide conjugates, HeLa and HEK 293 cells, respectively, were seeded in 8 well chamber slides (40 000 and 100 000 cells/well, respectively) and grown under standard growth conditions. Subconfluent cells were incubated with the double-labeled QD_{617}-[C^{17}]-hCT(18−32)-k7(CF) (0.02 μM QD) for 1.5 and 4 h. After 4 h incubation, the QD-hCT-peptide conjugate solution was removed and cell media were added. Fluorescence imaging was performed after 1.5, 4, and 24 h shortly after washing the cells 3−5 times with 200 μL HBSS (pH 7). At least 100 μL HBSS was added for fluorescence imaging that was performed using a Zeiss Axiovert 200 inverse phase-contrast fluorescence microscope provided with an ApoTome and a 63×/1.4 oil immersion objective.

Peptide-Mediated RNA Delivery. We complexed Cy-3-labeled RNAs of different lengths with QD_{514}-hCT-peptide conjugates: 83 base long RNA (5′-GGGAGAATTCCGACCA-GAAGAUUGAGAAGGGCGAUCUUCCGGCCGGACCUCA-ACCGGCGUAUGUGGCUCUACAUGGAUCCUCA-3′) and 101 base long RNA (sequence: 5′-GGAGCUCAGCCUUCA-CUGCCGGAGUGCAUUGUUGGCUGGGUGAUCGUGGU-GGAGACCUUACCCCUCUACGGGGGGGUGGAGGGCA-CCACGGUCGGAUCCAC-3′). Final concentrations at the cells were 0.4 μM RNA and QD_{514}-[C^{17}]-hCT(18−32)-k7 (0.04 μM QD) in 200 μL OptiMEM.

Prior to the peptide−RNA complexation, the RNA was de- and renatured. Therefore, the required volume of RNA stock solution was diluted with RNase- and DNase-free distilled water to a final volume of 10 μL, heated up to 70 °C for 5 min and slowly cooled down to room temperature. Then, the required volume of QD_{514}-[C^{17}]-hCT(18−32)-k7 solution was added and the noncovalent peptide−RNA complexation was carried out for 1 h at 37 °C. Afterward, preheated serum-free OptiMEM was added to reach a final volume of 200 μL. The QD-peptide-RNA solution was added to the cells and incubated for 1.5 and 6 h, respectively, at 37 °C. For nuclear staining, Hoechst 33342 was added to a final concentration of 5 μg/mL 10 min prior to the end of complex incubation. Finally, after 1.5 or 6 h the QD−peptide−RNA solution was removed and the cells were washed four times with 200 μL OptiMEM. 100 μL HBSS was added to the cells, and fluorescence microscopic imaging was performed as described above.

The influence of chloroquine was investigated as follows: prior to the addition of the QD−peptide−RNA solution, the cells were preincubated with 100 μL chloroquine (100 μM). After 1.5 h incubation, the QD−peptide−RNA solution was removed, and the cells were treated as described above.

RESULTS

Synthesis of QD-hCT-Peptide Conjugates. Peptides were coupled covalently to green (514 nm emission maximum, QD_{514}) and red (617 nm emission maximum, QD_{617}) emitting QDs. For efficient cell delivery, we incorporated the branched hCT-derivative hCT(18−32)-k7 on the surface of the QDs. We recently were able to show that this branched peptide was internalized very effectively in several cell lines (*21*). Furthermore, owing to the cationic sequence of the side chain an efficient complexation of negatively charged structures like oligonucleotides is possible. Synthesis of the QD−peptide conjugates was performed according to the manufacturer's protocol. Briefly, we first coupled the bifunctional cross-linker sulfo-SMCC to PEG-NH_2 functionalized QDs. Then, the peptide was introduced as [C^{17}]-hCT(18−32)-k7 that reacted selectively with the maleimide of the cross-linker (see Figure 1A for reaction scheme). We prepared QD−peptide conjugates with a QD to peptide ratio of 1:100 up to 1:300. Additionally, we synthesized a double-labeled conjugate where the peptide was labeled with 5(6)-carboxyfluorescein (CF) at the N-terminus of the side sequence k7 (see Figure 1B for details).

The coupling efficiency was determined by performing either a Bradford assay or, in the case of the double-labeled conjugate, by measuring the fluorescence of CF. For the red-emitting QDs, the assays revealed about 100 peptide molecules per quantum dot, whereas for the smaller green-emitting QDs, ratios of about 1:50 QD to peptide were determined.

Cellular Uptake in HeLa and HEK 293 Cells. Cellular uptake was studied in two different cell lines, HeLa and HEK

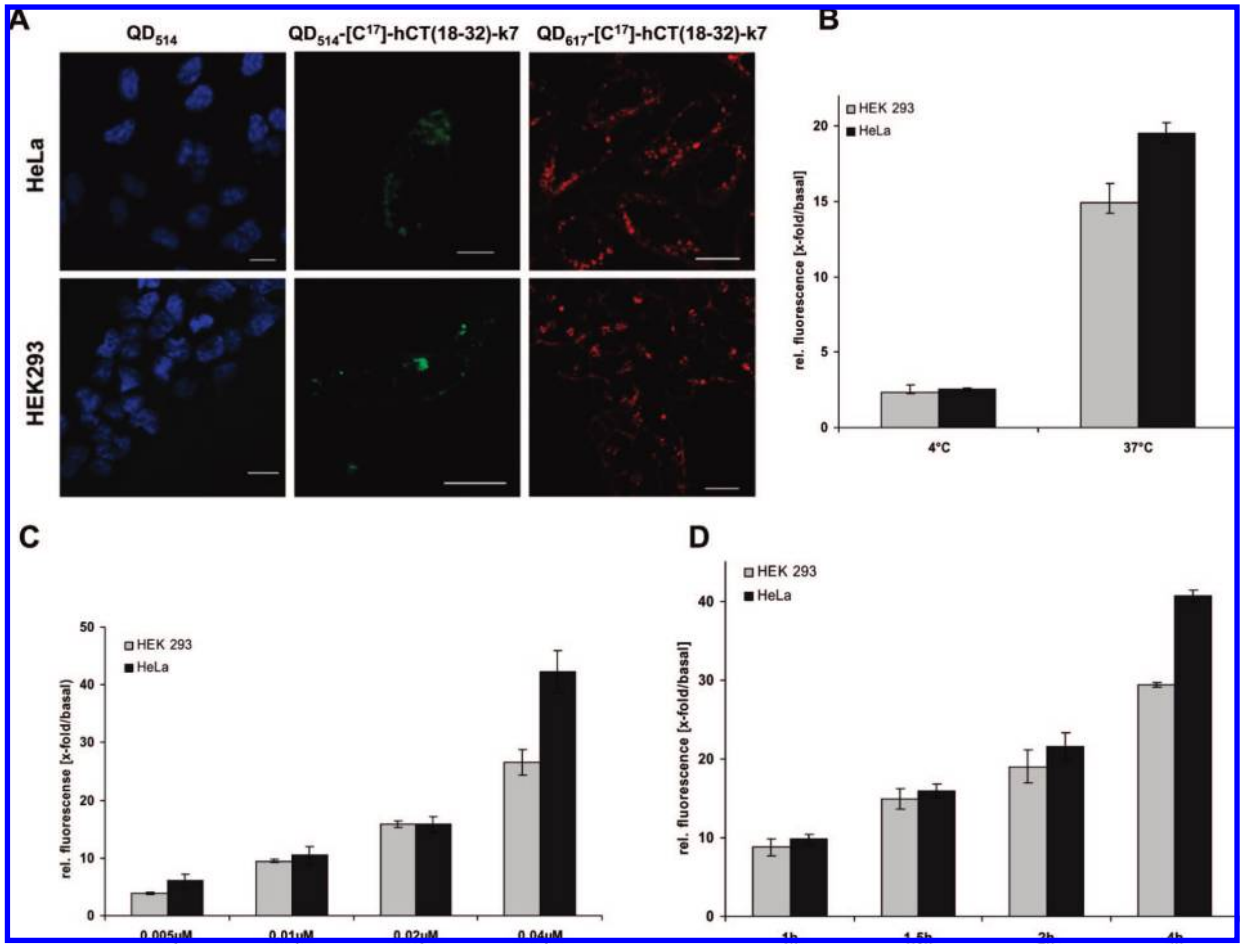

Figure 2. Internalization of QD−hCT carrier peptide conjugates in HeLa and HEK 293 cells. (A) Representative fluorescence microscopy images of QD_{514}-solution only (0.25 μM), QD_{514}-[C^{17}]-hCT(18−32)-k7 (0.04 μM QD concentration) and QD_{617}-[C^{17}]-hCT(18−32)-k7 (0.02 μM QD concentration). The scale bar is 20 μm. (B,C,D) Uptake of QD_{617}-[C^{17}]-hCT(18−32)-k7 (0.02 μM QD concentration) in HEK 293 and HeLa cells as determined by flow cytometry at either 37 or 4 °C for 90 min (B), at different concentrations for 90 min at 37 °C (C) and after incubation the cells up to 4 h at 37 °C.

293 cells, because these cell lines have often been used in recent reports (*6, 22, 23*). After incubation with nonconjugated QDs, we observed no detectable intracellular fluorescence, indicating that the nanoparticles were not able to enter the cells by themselves (shown for QD_{514} in Figure 2A). Cell internalization of the $QD_{617/514}$-[C^{17}]-hCT(18−32)-k7 conjugates was slow and occurred efficiently after 90 min of incubation. A punctuate and vesicular uptake pattern was observed in both cell lines pointing to an endocytotic entry pathway (Figure 2A). Subsequently, we studied in more detail the uptake of QD_{617}-[C^{17}]-hCT(18−32)-k7 conjugates in both cell lines by using flow cytometry. Uptake was significantly reduced at 4 °C (Figure 2B), supporting an energy-dependent internalization mechanism. This is in agreement with previously published results on QD−peptide delivery in both HEK 293 (*6*) and HeLa (*23*) cells. In addition, internalization of the QD−peptide bioconjugates is both concentration- (Figure 2C) and time-dependent (Figure 2D) in HEK 293 as well as in HeLa cells.

To get more insight into the entry mechanism, we investigated the uptake by the simultaneous delivery of AlexaFluor 488-conjugated cholera toxin subunit B (AF488-CtxB) or AlexaFluor 488-conjugated transferrin (AF488-Tf) into the cells. Like other microbial toxins, the active part of cholera toxin subunit B is internalized by an endocytosis pathway that is independent of clathrin and involves lipid rafts (*24, 25*). However, labeled transferrin is commonly used to monitor clathrin-dependent uptake in cells (*26*). Therefore, cells were preincubated with the appropriate marker, and subsequently, the QD−bioconjugates were added. We inspected the cells after 45 min, the time point at which we assumed that cell entry of the QD−peptide assemblies occurred. Figure 3A,B shows the uptake of QD_{617}-[C^{17}]-hCT(18−32)-k7 conjugates in HeLa cells. No colocalization was found for QD−peptide conjugates and AF488-Tf, whereas after incubation with AF488-CtxB, colocalization of internalized QD−peptide conjugate and CtxB was evident as seen by the merged fluorescence on the plasma membrane. Quite different results were obtained after incubating HEK 293 cells with the QD−peptide conjugate and the two endocytosis markers (Figure 3C,D). Here, no colocalization within the cell was observed. Moreover, it seems that the entry of the markers into this cell line occurs very fast, while the QD−peptide conjugate is mostly present on the plasma membrane and only to a minor fraction in the cell interior. Even after inspecting the cells at different time points (15, 30, 60, 90, 120 min), we did not detect any degree of overlap in the fluorescence pattern (data not shown).

Inhibition of Endocytotic Pathways. To further characterize the uptake mechanism of the QD−peptide bioconjugates, we preincubated HeLa as well as HEK 293 cells with different inhibitors interfering with individual endocytotic pathways (*25*−*30*). After 30 min preincubation with these different inhibitors, we analyzed the cellular uptake of the QD−peptide conjugates (cells were incubated with bioconjugates for 90 min) by flow cytometry. Additionally, we tested the influence of the same inhibitors on the uptake of 5(6)-carboxyfluorescein (CF)-labeled hCT(18−32)-k7 in both cell lines to get some insights into the

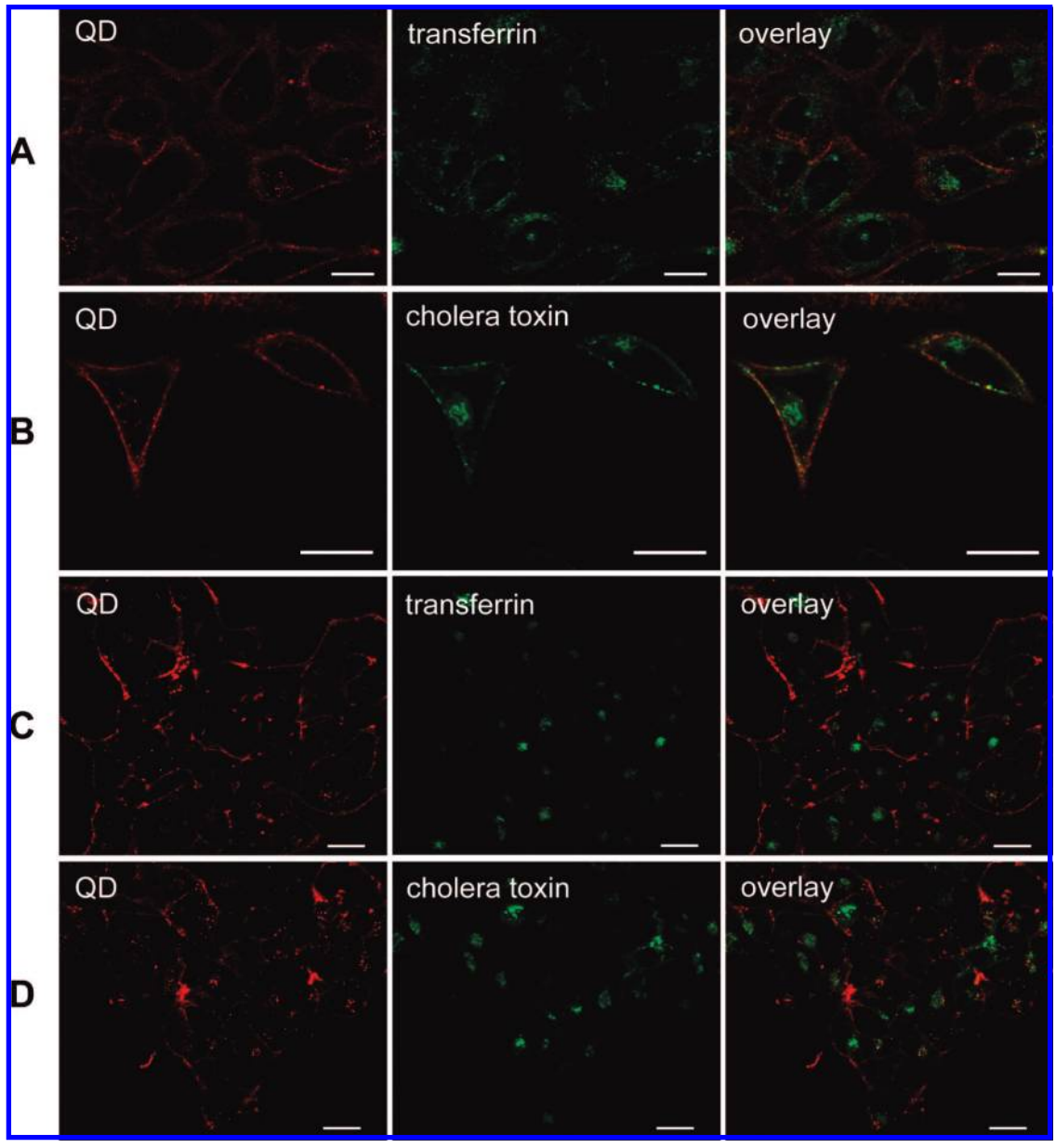

Figure 3. Colocalization study of QD_{617}-[C^{17}]-hCT(18−32)-k7 in HeLa (A,B) and HEK 293 (C,D) with transferrin or cholera toxin, respectively. Colocalized vesicels are visible in yellow, QD_{617}-[C^{17}]-hCT(18−32)-k7 conjugate in red, and endocytosis markers (transferrin and cholera toxin) in green. For colocalization studies with transferrin, cells were incubated with QD_{617}-[C^{17}]-hCT(18−32)-k7 and simultaneously stained with 50 μg/mL Alexa Fluor 488-conjugated transferrin for 45 min at 37 °C (A,C). For colocalization studies with Alexa Fluor 488-conjugated cholera toxin, cells were preincubated with 10 μg/mL cholera toxin at 4 °C, and the marker was then replaced by QD_{617}-[C^{17}]hCT(18−32)-k7 for 1 h at 37 °C (B,D). The scale bar is 20 μm.

influence of the cargo size on the internalization process. Unspecific bound peptides were detached from the outer leaflet of the cell membrane by trypsin digestion. Figure 4A,B demonstrates the uptake of QD_{617}-[C^{17}]-hCT(18−32)-k7 and CF-hCT(18−32)-k7 in HeLa and HEK 293 cells, respectively. We found out that the uptake of the QD−peptide conjugate in HeLa cells seems to follow two different pathways (see Figure 4A). The decreased uptake after depletion of cholesterol through MβCD proves the results from the colocalization studies and points to a lipid raft-dependent entry pathway. The second way is obviously mediated by macropinocytosis, a fact that is indicated by the influence of 5-(*N*-ethyl-*N*-isopropyl)amiloride (EIPA). Interestingly, the uptake of CF-hCT(18−32)-k7 is realized by a third pathway in HeLa cells that is clathrin-dependent. Upon preincubation with chlorpromazine, a marker that inhibits this endocytosis pathway, the uptake was decreased (see Figure 4A). The same pathways seem to be involved in the internalization process of CF-hCT(18−32)-k7 in HEK 293 cells (see Figure 4B). Surprisingly, the uptake of QD_{617}-[C^{17}]-hCT(18−32)-k7 was not negatively influenced after preincubating HEK 293 cells with any of the tested inhibitors. In contrast, here we observed an increase in uptake (see Figure 4B).

To eliminate influence of the tested inhibitors on cell viability and thus impair the results of the inhibition studies, we performed resazurin-based cell viability assays. As demonstrated in Figure 4C, the impact of the inhibitors on cell viability was negligible for HeLa as well as for HEK 293 cells in the tested concentration range.

Stability. By using the double-labeled compound, we investigated the stability of the QD−peptide bioconjugates after cell entry. Hence, we incubated HeLa and HEK 293 cells for 24 h with the conjugate QD_{617}-[C^{17}]-hCT(18−32)-k7(CF) and visualized the cells by fluorescence microscopy after 1.5, 4, and 24 h.

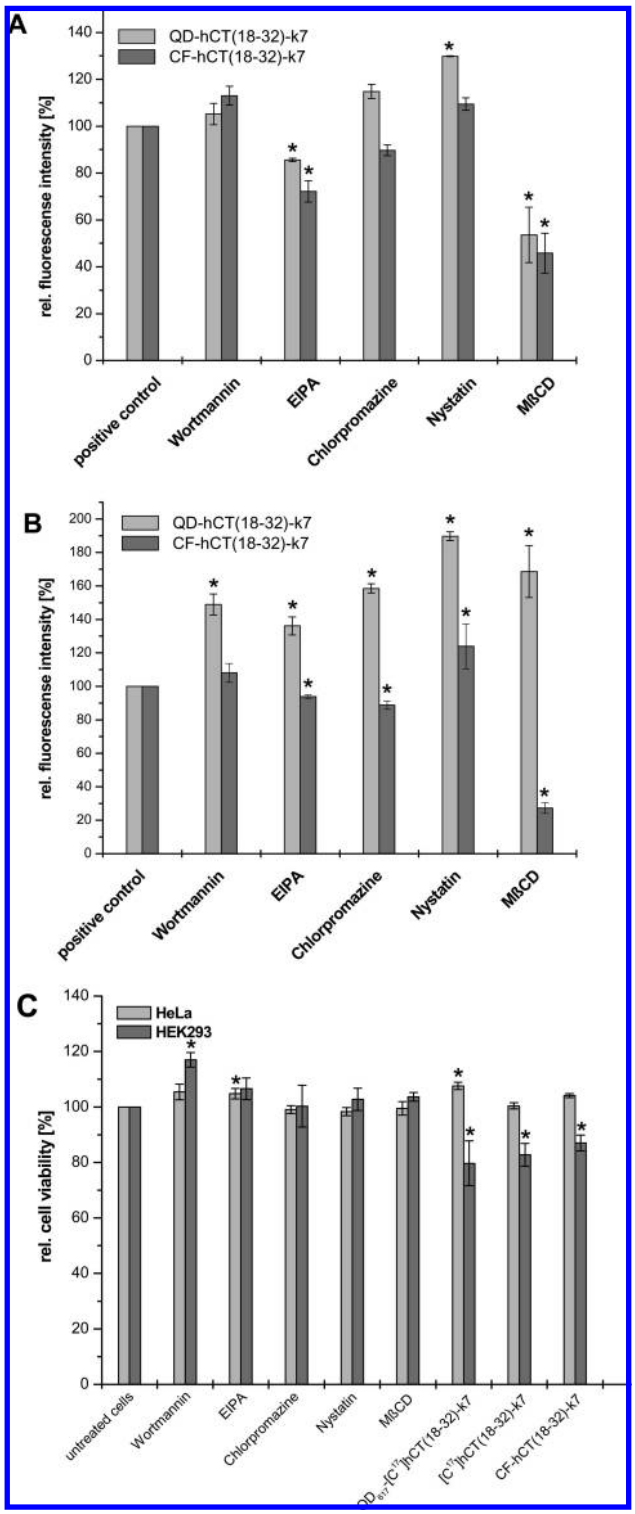

Figure 4. Endocytosis inhibition and toxicity studies. Panels A and B show uptake and endocytosis inhibition of CF-hCT(18−32)-k7 and QD_{617}-[C^{17}]-hCT(18−32)-k7 in HeLa (A) and HEK 293 (B) cells as determined by flow cytometry. The inhibition of endocytosis was performed by pretreating cells with 200 nM wortmannin, 100 μM EIPA, 20 μM chlorpromazine, 27 μM nystatin, and 10 mM methyl-β-cyclodextrin (MβCD) before incubation with QD_{617}-[C^{17}]-hCT(18−32)-k7 (0.02 μM QD) for 90 min or 20 μM CF-hCT(18−32)-k7 for 60 min. Cells incubated only with peptide or QD−peptide conjugate were used as control cells and set as 100%. Panel C shows relative cell viability of HeLa and HEK 293 cells after treatment with inhibitor for 60 min and peptide or QD−peptide solutions for 24 h (for details, see Experimental Section). Data are normalized to untreated cells (100% viability). Means were compared using Student's *t* test. A *P* value of <0.05 was considered significant and is indicated by an asterisk symbol (*).

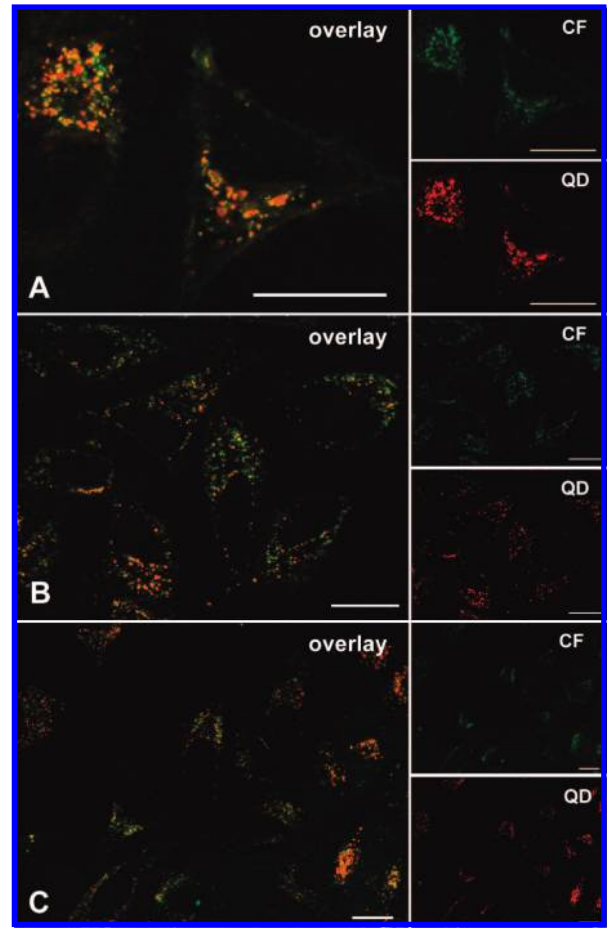

Figure 5. Stability of the new QD−hCT−peptide bioconjugates in HeLa cells. Colocalized vesicles are visible in yellow, carboxyfluorescein in green, and QDs in red. Cells were incubated with the double-labeled conjugate QD_{617}-[C^{17}]-hCT(18−32)-k7(CF) (0.02 μM QD concentration) for 1.5 h (Panel A) or 4 h (Panel B), and fluorescence imaging was performed at 1.5 h (Panel A), 4 h (Panel B), and 24 h (Panel C). The scale bar is 20 μm.

The merged fluorescence of the two fluorophors even after 24 h demonstrates that the conjugate seemed to be mostly intact (see Figure 5 for HeLa cells). In addition, it can be seen that the peptide-labeled nanoparticles were still entrapped in vesicles. The same results were obtained for HEK 293 cells (see Supporting Information Figure 2).

Furthermore, potential cytotoxic effects of the QD-CPP assemblies were assessed using a cell proliferation assay. The results confirmed no influence on cell viability for the QD−peptide conjugates in HeLa cells relative to untreated control cells (see Figure 4C). In contrast, cell viability was slightly reduced to 80% after incubating HEK 293 cells with the conjugate for 24 h.

Cargo Delivery. The main focus of this study was to create multifunctional particles for both imaging and transport of bioactive molecules. A major difference between this work and earlier studies is that the conjugated carrier peptides simultaneously function for the delivery of both the QD and an attached cargo. Furthermore, by complexing the cargo directly to the carrier peptide our approach circumvents the tradeoffs in the number of attached species on the QD surface. Since negatively charged oligonucleotides are not able to translocate the cell membrane by themselves, there is a great demand on effective delivery systems for siRNA or aptamers in gene regulation strategies. Therefore, as proof of our concept, we chose to transport Cy-3 labeled RNA into HeLa and HEK 293 cells. The Cy-3 label served for visualizing the fate of the cargo after cell

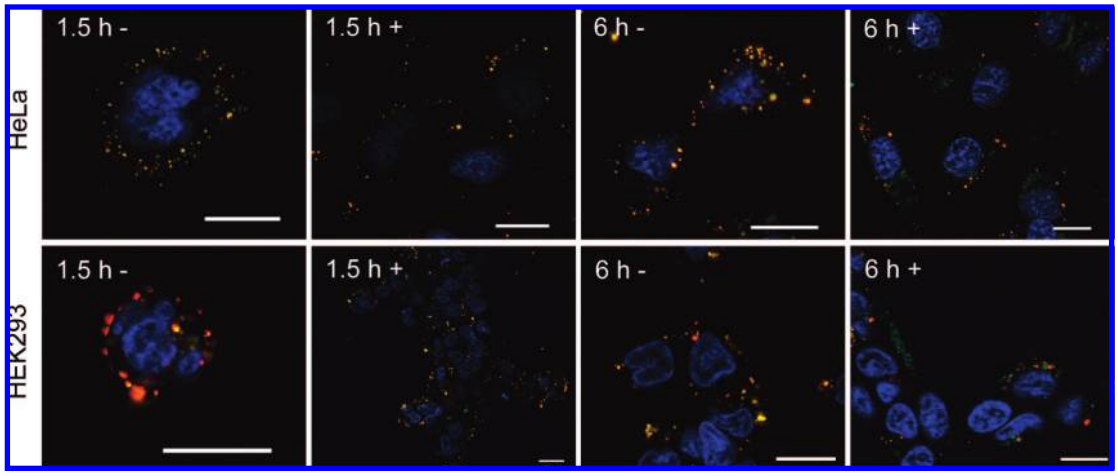

Figure 6. RNA delivery mediated by the QD_{514}-[C^{17}]-hCT(18−32)-k7 bioconjugate. Delivery of the 83 base long RNA in HeLa and HEK 293 cells. Colocalization is visible in yellow, Cy-3 labeled RNA in red, QD_{514}-[C^{17}]-hCT(18−32)-k7 in green, and the nucleus was stained with Hoechst 33342 in blue. The cells were incubated with QD-peptide-RNA either for 1.5 h (1.5 h -) or 6 h (6 h -). The influence of the pretreatment with 100 μM chloroquine for 1 h is shown in panels marked with +. The scale bar is 20 μm.

entry. Thus, we complexed QD_{514}-[C^{17}]-hCT(18−32)-k7 with RNAs of different lengths (either 83 or 101 bases long).

One major problem when using CPP for cargo delivery is their enclosure in endosomes after cell entry. The results from our internalization studies clearly showed entrapment of the QD−peptide conjugates in vesicles that may be endosomes or lysosomes. To overcome this difficulty, we also treated the cells with the antimalaria drug chloroquine. This cell-permeable base is described to neutralize the acidic environment in the endosomes leading to reduction of endolysosomal hydrolytic degradation and destabilization of the complex between carrier and cargo (*31*). Figure 6 shows HeLa (upper row) and HEK 293 (lower row) cells after incubation of complexes formed from QD_{514}-[C^{17}]-hCT(18−32)-k7 and the 83 base long RNA. Cells were inspected after 1.5 and 6 h. As described above, cellular distribution was monitored in preparations with or without the addition of chloroquine. It is evident that the complex is still intact after 6 h in both cell lines, whereas upon the addition of chloroquine, most of the substances have distributed into the cytoplasma. Only the green fluorescence coming from the QD−peptide conjugates was visible. The red fluorescence from the RNA was only merely seen. Therefore, we conclude that the RNA must have been detached from the complex with the peptides coupled to the QD surface. The same results were obtained after incubation of complexes formed from QD_{514}-[C^{17}]-hCT(18−32)-k7 and the 101 base long RNA in both tested cell lines (data not shown).

DISCUSSION

Over the past two decades there has emerged an immense interest in quantum dots as fluorescent probes for biomolecular and cell imaging owing to their unique spectroscopic properties. Several examples are now available demonstrating successful *in vitro* and *in vivo* applications of QDs in tissue staining and cell labeling. Here, different strategies for cell internalization have been followed, like nonspecific or specific binding to the cell surface or the use of antibody-coated QDs (*32, 33*). Another promising approach for realizing effective cell uptake is the attachment of cell-penetrating peptides to the QD surface. This class of peptides is able to penetrate the cell membrane in a receptor-independent way and shuttle various cargoes into the cell at the same time. Recent advances have shown the applicability of CPP in an impressive mode, and until now, a series of different biomolecules has been successfully transported into diverse cell lines. Nevertheless, only a few studies exist that have investigated peptide-coated quantum dots especially for their stability, toxicity, and internalization mechanism. Recently, Ruan et al. published data concerning cellular uptake and intracellular fate of Tat-functionalized QDs (*23*). They observed an engulfment of Tat-QDs in vesicles where they were bound to the inner membrane, and the subsequent transport of these vesicles to the perinuclear region. Furthermore, they found vesicles loaded with Tat-QDs on the outer membrane resulting from vesicle shedding. Moreover, it was assumed that the Tat peptide-conjugated QDs are internalized by macropinocytosis. Another paper from the same group dealt with PEG/PEI-coated QDs. Herein, the authors could show an improvement concerning the escape from intracellular acidic organelles (*34*). A general major drawback in such applications is, however, the toxicity of PEI that was minimized in this study by grafted PEG segments.

Our work focused on the development of transport systems that contain photostable markers like QDs and are useful as fluorescent probes for imaging, tracking, and delivery purposes. Furthermore, we were interested in the stability and toxicity of the new constructs and their internalization mechanism. Therefore, we generated different QD−peptide bioconjugates by attaching cysteine-modified [C^{17}]-hCT(18−32)-k7 to the surface of PEG-coated QD. We also synthesized a double-labeled compound by coupling [C^{17}]-hCT(18−32)-k7(CF) to red emitting QD_{617}. By measuring the fluorescence of the second fluorophor CF and comparing it with a calibration curve, it was possible to determine the amount of peptides per QD_{617} to a ratio of about 100:1. In our experiments, this value barely differed from the one we obtained by Bradford assay. Generally, this ratio is in good agreement with values obtained in previous studies where peptides were attached on a QD surface (*11*). Moreover, by introducing a second fluorophor the determination of the amount of peptides on the QD surface is achieved in an easy way. Thus, long-time stability can simply be monitored. We determined that the double-labeled QD−peptide conjugate was stable at least over a period of one year (data not shown). A similar approach to quantify the number of peptides attached per QD was adopted by Derfus et al. (*35*). The disulfide bond of a cleavable cross-linker between FITC-labeled peptides and nanoparticles was reduced by 2-mercaptoethanol and the amount of FITC-labeled peptide was then quantified by fluorescence. However, our approach differs from other strategies where the therapeutic and delivery entities are simultaneously attached to

the QD surface. Thus, our newly formed constructs can directly serve as delivery and imaging tools.

Next, we analyzed the uptake and distribution of our QD−peptide conjugates in two cell lines, HEK 293 and HeLa. The first internalization experiments using fluorescence microscopy showed that the generated bioconjugates were able to cross the lipid barrier of the cells. Both HeLa and HEK 293 cells efficiently took up the peptide-coated QDs. Also, we detected no uptake of the QDs alone. This is in agreement with the study of Delehanty et al. on self-assembled quantum dot−peptide bioconjugates (*6*). Furthermore, the vesicular distribution pattern suggests an endocytotic mechanism. This was confirmed by investigating the uptake of QD_{617}-[C^{17}]-hCT(18−32)-k7 using flow cytometry. We found that uptake is reduced at 4 °C pointing to an energy-dependent internalization. Additionally, internalization of the studied QD−peptide conjugates is concentration- and time-dependent. Interestingly, these results were similar to previous studies using carboxyfluorescein (CF)-labeled hCT-derived peptides (*22*). In addition, recent studies on HEK 293 cells revealed that the uptake of CF-hCT(18−32)-k7 is temperature-, concentration-, and time-dependent. Here, it was also found that the uptake could not be displaced by the addition of unlabeled hCT(18−32)-k7 peptide, pointing to a receptor-independent uptake mechanism (*36*).

Accordingly, we studied the uptake in more detail because CPP are known to use several endocytotic pathways for cell internalization. For instance, most of the cationic peptides investigated so far enter the cells via clathrin-independent pathways including macropinocytosis (*37*−*39*). Therefore, we started with colocalization experiments by using fluorescent-labeled transferrin and cholera toxin subunit B to distinguish at first between clathrin-dependent (transferrin) and lipid raft-dependent (CTxB) endocytosis. Since we were interested in the processes of cell entry, we inspected the cells to an early stage, after 45 min, when most of the QD−peptide bioconjugates were passing the cell membrane, and only few constructs stayed inside the cell. From fluorescence imaging studies of HeLa cells incubated with QD_{617}-[C^{17}]-hCT(18−32)-k7 and AlexaFluor 488 labeled CTxB, we assume a lipid raft dependent uptake mechanism due to clear colocalization of both substances. It is known that HeLa cells have decreased caveolin-1 expression. Therefore, internalization of cholera toxin subunit B can occur via the clathrin-mediated pathway, too, but it was found out that the significant fraction is internalized via clathrin-independent pathways (*40*−*42*). For HEK 293 cells, the results were not as clear, since we could not detect any colocalization of our QD−peptide conjugates with neither transferrin nor CTxB. In both cases, the marker was very rapidly taken up by HEK 293 cells. However, we were additionally interested in the influence of the cargo size on the internalization process and compared the results of the QD−peptide bioconjugates to the uptake of CF-labeled hCT(18−32)-k7. In contrast to the QD−peptide conjugate, we detected colocalization with both markers transferrin and CTxB in HeLa cells (see Supporting Information Figure 1) indicating that CF-hCT(18−32)-k7 is internalized by both clathrin-dependent and -independent pathways. Again, we observed no colocalization after incubating HEK 293 cells with the peptides and either transferrin or CTxB.

Therefore, we decided to extend our studies by using several endocytotic inhibitors. We preincubated the cells with inhibitors for clathrin-dependent and -independent pathways, as well as for caveolin-dependent endocytosis and macropinocytosis. Our results show that the import of the conjugates was never fully blocked after preincubation with the inhibitors. Besides, we did not find any influence of wortmannin. Since wortmannin is reported to also affect the sorting pathways like recycling and degradation, it may have happened that internalization per se was not reduced but the fate of the peptides inside the cells was influenced. This has to be investigated further.

For HeLa cells, we conclude that the QD−peptide−bioconjugates appear to enter by macropinocytosis and lipid raft-dependent pathways. We could assess a strong influence of methyl-β-cyclodextrin (MβCD) to the amount of intracellular fluorescence. MβCD perturbs the function and organization of lipid rafts and is therefore a marker for raft processes. The results from the colocalization studies were consistent with this observation because they demonstrated simultaneous entrapment of hCT-QDs and cholera toxin subunit B also pointing to a lipid raft-dependent pathway. By using the inhibitor 5-(*N*-ethyl-*N*-isopropyl)amiloride (EIPA), the uptake of the bioconjugate was to some extent reduced as well, indicating that the internalization of the conjugate may occur by a second pathway that is macropincocytosis. Interestingly, when treating with the inhibitors we did not detect any decrease in uptake for the peptide-coated QDs in HEK 293 cells. Moreover, the inhibition of the pathways led to a dramatic increase in uptake in all cases. Recently, this effect was also reported by Duchardt et al. They detected a high increase in cellular fluorescence (4- to 7-fold) by flow cytometry after treatment with MβCD. They explained this observation on the one hand with the strong enrichment of the tested peptides at the plasma membrane. This fraction was also resistant to trypsin digestion (*38*). On the other hand, it may be that the inhibitors promote the uptake leading then to a more rapid internalization pathway. This could also be the case for the internalization of the QD−peptide conjugates in HEK 293 cells. Another explanation could be the retention of the QD−peptide conjugate inside the endosomal compartment and thus an inhibition of the rapid exit of its fragments out of the cytosol. Since we determined no relevant cytotoxicity for all tested inhibitors in the evaluated concentration range, we exclude the possibility that the increased uptake observed is due to any negative influence on cell viability.

In contrast, the CF-labeled peptide seemed to follow three different entry pathways in HeLa and HEK 293 cells. Additionally, the evaluation of the inhibition studies demonstrated strong evidence that EIPA, chlorpromazine, and MβCD influence the uptake. In HeLa cells, this is consistent with the observations we made by fluorescence microscopy where colocalization was found with fluorescent-labeled transferrin as well as with cholera toxin subunit B, pointing to both clathrin-dependent and -independent endocytosis. In addition, we detected reduced peptide uptake in the dependence of the particular inhibitors tested. Therefore, we assume that the most dominant entry pathway is lipid raft-dependent and that only a minor fraction of CF-hCT(18−32)-k7 peptides are internalized by clathrin-mediated endocytosis or macropinocytosis. The strong influence of MβCD to the uptake of CF-hCT(18−32)-k7 in HEK 293 cells is in our opinion not remarkable, since it is known that depletion of cholesterol can generally affect most of the endocytotic uptake pathways (*43*).

Interestingly, it seems that both tested substances labeled with cargoes of different sizes use more than one entry pathway. However, regarding the relatively high concentrations that are normally used to study CPP it is likely that the peptides enter through multiple pathways, i.e., fluid phase or nonspecific adsorptive endocytosis. In fact, Duchardt et al. concluded that peptide concentration is a key experimental condition when analyzing peptide uptake (*38*). In another study, it was hypothesized that, in HeLa cells, macropinocytosis operates at a low basal rate. Thus, an inhibition of clathrin- and caveolae-mediated pathways could result in the stimulation of macropinocytosis (*44*). However, the differences in the uptake of the QD−peptide conjugates concerning HEK 293 and HeLa cells could be explained on one hand by the involvement of a yet unknown

uptake pathway in HEK 293 cells. On the other hand, there is general disagreement regarding to what extent the exact uptake pathway can be elucidated by inhibition studies. This is because the sensitivity of a certain cell line to various inhibitors of endocytic uptake pathways is different. In fact, the results of these studies can only give some indication of how the uptake of a certain molecule or complex could happen. Nevertheless, in conclusion, our findings contribute to the understanding of how CPP and especially hCT-derived carrier peptides are able to enter the cell interior and how the attached cargo can influence the adopted pathway. Anyway, the dissection of such mechanistic aspects is crucial in the further development and application of such drug delivery vectors for pharmaceutical purposes.

Furthermore, we demonstrated that our newly developed QD-CPP assemblies exert no cytotoxic effects on HeLa cells and have only a minor influence on cell viability after incubation of HEK 293 cells for 24 h with the constructs. This could be due to aggregation of the QD−peptide conjugates after 24 h in the cell interior. The toxic influence of the CF-hCT(18−32)-k7 peptides may be due to their rapid internalization in this cell line (as observed by fluorescence microscopy), an effect that was also described by Delehanty et al. (*6*). Furthermore, we assessed the stability of the QD−peptide nanoparticles after exposure of the double-labeled QD−peptide conjugate for 24 h to both cell-lines. Still after 24 h, the constructs of QD and peptide seemed to be mostly intact, as indicated by the merged fluorescence. From this, we conclude that the QD surface can effectively help to protect the peptides from degradation. Considering future *in vivo* applications, this could be important because one major drawback in using peptides is often the lack of metabolic stability that restricts many *in vivo* experiments.

The past years have sparked great interest in the therapeutic potential of gene regulation and gene silencing. As a result, there have been great efforts in the development of different strategies to deliver siRNA or aptamers into mammalian cells. The aim of this work was therefore to provide tools that are not only helpful in imaging but also in drug delivery applications. According to this, our results from the delivery studies with Cy-3 labeled RNA demonstrate the versatility of our peptide−QD conjugates. RNA of different length was efficiently transported into HeLa and HEK 293 cells. Furthermore, with the help of chloroquine it was possible to deliver the conjugates into the cytosol. Recently, we were able to demonstrate that the addition of chloroquine is useful in improving transfection rates in several cell lines and does not influence cell viability in the tested concentrations (*21*). Other approaches like the addition of cationic lipids are common for achieving endosomal escape (*35*). However, depending on whether chloroquine was added or not the complex of QD−peptide conjugates and RNA persisted in vesicles or was discharged in the cytoplasma. Interestingly, upon release out of the vesicles it seems that the RNA has dissociated from the QD−peptide assembly. After 6 h, only the green fluorescence was visible in the cytosol originating from the QD-bioconjugate. The red fluorescence from the RNA was only merely seen. Therefore, it must be assumed that the RNA dissociated from the positively charged peptides coupled to the QDs. Since we could show that the QD−peptide conjugate was stable for at least 24 h, the green fluorescence is in fact assumed to derive from the intact QD−peptide bioconjugate. The problem in the use of QDs is that they are sequestered in vesicles after cell entry. Thus, they are not available for molecular recognition or targeting. By using our approach, this obstacle can be overcome, and the delivery of therapeutic RNA to its target can be realized. Therefore, our delivery systems could be very useful tools for the transport and monitoring of other structures like siRNA or aptamers.

CONCLUSION

The aim of this study was to develop fluorescent nanoparticles suitable for the nonviral delivery and monitoring of therapeutic oligonucleotides. Therefore, we incorporated in a first step hCT-derived carrier peptides on the surface of luminescent quantum dots. Second, we carefully characterized these new systems and could demonstrate that they are nontoxic and possess high stability inside cells. Furthermore, we found some key factors concerning their uptake mechanism. The last step demonstrated that our QD−peptide conjugates successfully deliver complexed RNA into cells. This explored approach could be easily adapted to the transport and tracking of other biologically active molecules important in gene therapy.

ACKNOWLEDGMENT

The authors thank R. Reppich-Sacher for recording the MALDI mass spectra and K. Löbner for help in cell culture experiments. Cy-3 labeled RNA was a gift from Prof. Dr. U. Hahn and is kindly acknowledged. I. Neundorf thanks Prof. Dr. A. G. Beck-Sickinger for generous access to all resources of the institute.

Supporting Information Available: Supplementary experimental figures and description of the figures. This material is available free of charge via the Internet at http://pubs.acs.org.

LITERATURE CITED

(1) Jaiswal, J. K., Mattoussi, H., Mauro, J. M., and Simon, S. M. (2003) Long-term multiple color imaging of live cells using quantum dot bioconjugates. *Nat. Biotechnol. 21*, 47–51.

(2) Smith, A. M., and Nie, S. (2004) Chemical analysis and cellular imaging with quantum dots. *Analyst 129*, 672–677.

(3) Watson, A., Wu, X., and Bruchez, M. (2003) Lighting up cells with quantum dots. *Biotechniques 34*, 296300, 302−303.

(4) Mae, M., and Langel, U. (2006) Cell-penetrating peptides as vectors for peptide, protein and oligonucleotide delivery. *Curr. Opin. Pharmacol. 6*, 509–514.

(5) Snyder, E. L., and Dowdy, S. F. (2005) Recent advances in the use of protein transduction domains for the delivery of peptides, proteins and nucleic acids in vivo. *Expert Opin. Drug Delivery 2*, 43–51.

(6) Delehanty, J. B., Medintz, I. L., Pons, T., Brunel, F. M., Dawson, P. E., and Mattoussi, H. (2006) Self-assembled quantum dot-peptide bioconjugates for selective intracellular delivery. *Bioconjugate Chem. 17*, 920–927.

(7) Lagerholm, B. C., Wang, M., Ernst, L. A., Ly, D. H., Liu, H., Bruchez, M. P., and Waggoner, A. S. (2004) Multicolor coding of cells with cationic peptide coated quantum dots. *Nano Lett. 4*, 2019–2022.

(8) Bendifallah, N., Rasmussen, F. W., Zachar, V., Ebbesen, P., Nielsen, P. E., and Koppelhus, U. (2006) Evaluation of cell-penetrating peptides (CPPs) as vehicles for intracellular delivery of antisense peptide nucleic acid (PNA). *Bioconjugate Chem. 17*, 750–758.

(9) Pooga, M., Kut, C., Kihlmark, M., Hallbrink, M., Fernaeus, S., Raid, R., Land, T., Hallberg, E., Bartfai, T., and Langel, U. (2001) Cellular translocation of proteins by transportan. *Faseb J. 15*, 1451–1453.

(10) Turner, J. J., Arzumanov, A. A., and Gait, M. J. (2005) Synthesis, cellular uptake and HIV-1 Tat-dependent trans-activation inhibition activity of oligonucleotide analogues disulphide-conjugated to cell-penetrating peptides. *Nucleic Acids Res. 33*, 27–42.

(11) Akerman, M. E., Chan, W. C., Laakkonen, P., Bhatia, S. N., and Ruoslahti, E. (2002) Nanocrystal targeting in vivo. *Proc. Natl. Acad. Sci. U.S.A. 99*, 12617–12621.

(12) Lewin, M., Carlesso, N., Tung, C. H., Tang, X. W., Cory, D., Scadden, D. T., and Weissleder, R. (2000) Tat peptide-derivatized magnetic nanoparticles allow in vivo tracking and recovery of progenitor cells. *Nat. Biotechnol. 18*, 410–414.

(13) Pontiroli, A. E., Alberetto, M., and Pozza, G. (1985) Intranasal calcitonin and plasma calcium concentrations in normal subjects. *Br. Med. J. (Clin. Res. Ed.) 290*, 1390–1391.

(14) Stroop, S. D., Nakamuta, H., Kuestner, R. E., Moore, E. E., and Epand, R. M. (1996) Determinants for calcitonin analog interaction with the calcitonin receptor N-terminus and transmembrane-loop regions. *Endocrinology 137*, 4752–4756.

(15) Neundorf, I., and Beck-Sickinger, A. G. (2005) Calcitonin-derived carrier peptides. *Curr. Pharm. Des. 11*, 3661–3669, Calcitonin-derived carrier peptides.

(16) Krauss, U., Kratz, F., and Beck-Sickinger, A. G. (2003) Novel daunorubicin-carrier peptide conjugates derived from human calcitonin segments. *J. Mol. Recognit. 16*, 280–287.

(17) Machova, Z., Muhle, C., Krauss, U., Trehin, R., Koch, A., Merkle, H. P., and Beck-Sickinger, A. G. (2002) Cellular internalization of enhanced green fluorescent protein ligated to a human calcitonin-based carrier peptide. *ChemBioChem 3*, 672–677.

(18) Rennert, R., Wespe, C., Beck-Sickinger, A. G., and Neundorf, I. (2006) Cell-penetrating peptides as vectors for peptide, protein and oligonucleotide delivery. *Biochim. Biophys. Acta 1758*, 347–354.

(19) Rennert, R., Neundorf, I., and Beck-Sickinger, A. G. (2008) Calcitonin-derived peptide carriers: mechanisms and application. *Adv. Drug Delivery Rev. 60*, 485–498.

(20) Krauss, U., Muller, M., Stahl, M., and Beck-Sickinger, A. G. (2004) In vitro gene delivery by a novel human calcitonin (hCT)-derived carrier peptide. *Bioorg. Med. Chem. Lett. 14*, 51–54.

(21) Rennert, R., Neundorf, I., Jahnke, H. G., Suchowerskyj, P., Dournaud, P., Robitzki, A., and Beck-Sickinger, A. G. (2008) Generation of carrier peptides for the delivery of nucleic acid drugs in primary cells. *ChemMedChem 3*, 241–253.

(22) Foerg, C., Ziegler, U., Fernandez-Carneado, J., Giralt, E., Rennert, R., Beck-Sickinger, A. G., and Merkle, H. P. (2005) Decoding the entry of two novel cell-penetrating peptides in HeLa cells: lipid raft-mediated endocytosis and endosomal escape. *Biochemistry 44*, 72–81.

(23) Ruan, G., Agrawal, A., Marcus, A. I., and Nie, S. (2007) Imaging and tracking of Tat peptide-conjugated quantum dots in living cells: new insights into nanoparticle uptake, intracellular transport, and vesicle shedding. *J. Am. Chem. Soc. 129*, 14759–14766.

(24) Nichols, B. J., Kenworthy, A. K., Polishchuk, R. S., Lodge, R., Roberts, T. H., Hirschberg, K., Phair, R. D., and Lippincott-Schwartz, J. (2001) Rapid cycling of lipid raft markers between the cell surface and Golgi complex. *J. Cell Biol. 153*, 529–541.

(25) Puri, V., Watanabe, R., Singh, R. D., Dominguez, M., Brown, J. C., Wheatley, C. L., Marks, D. L., and Pagano, R. E. (2001) Clathrin-dependent and -independent internalization of plasma membrane sphingolipids initiates two Golgi targeting pathways. *J. Cell Biol. 154*, 535–547.

(26) Thorstensen, K., and Romslo, I. (1988) Uptake of iron from transferrin by isolated rat hepatocytes. A redox-mediated plasma membrane process? *J. Biol. Chem. 263*, 8844–8850.

(27) Shpetner, H., Joly, M., Hartley, D., and Corvera, S. (1996) Potential sites of PI-3 kinase function in the endocytic pathway revealed by the PI-3 kinase inhibitor, wortmannin. *J. Cell Biol. 132*, 595–605.

(28) Swanson, J. A., and Watts, C. (1995) Macropinocytosis. *Trends Cell Biol. 5*, 424–428.

(29) Le, P. U., and Nabi, I. R. (2003) Distinct caveolae-mediated endocytic pathways target the Golgi apparatus and the endoplasmic reticulum. *J. Cell Sci. 116*, 1059–1071.

(30) Ikonen, E. (2001) Roles of lipid rafts in membrane transport. *Curr. Opin. Cell Biol. 13*, 470–477.

(31) Cheng, J., Zeidan, R., Mishra, S., Liu, A., Pun, S. H., Kulkarni, R. P., Jensen, G. S., Bellocq, N. C., and Davis, M. E. (2006) Structure-function correlation of chloroquine and analogues as transgene expression enhancers in nonviral gene delivery. *J. Med. Chem. 49*, 6522–6531.

(32) Zhou, M., Nakatani, E., Gronenberg, L. S., Tokimoto, T., Wirth, M. J., Hruby, V. J., Roberts, A., Lynch, R. M., and Ghosh, I. (2007) Peptide-labeled quantum dots for imaging GPCRs in whole cells and as single molecules. *Bioconjugate Chem. 18*, 323–332.

(33) Wu, X., Liu, H., Liu, J., Haley, K. N., Treadway, J. A., Larson, J. P., Ge, N., Peale, F., and Bruchez, M. P. (2003) Immunofluorescent labeling of cancer marker Her2 and other cellular targets with semiconductor quantum dots. *Nat. Biotechnol. 21*, 41–46.

(34) Duan, H., and Nie, S. (2007) Cell-penetrating quantum dots based on multivalent and endosome-disrupting surface coatings. *J. Am. Chem. Soc. 129*, 3333–3338.

(35) Derfus, A. M., Chen, A. A., Min, D. H., Ruoslahti, E., and Bhatia, S. N. (2007) Targeted quantum dot conjugates for siRNA delivery. *Bioconjugate Chem. 18*, 1391–1396.

(36) Rennert, R., Neundorf, I., Beck-Sickinger, A. G. (2007) Synthesis and application of peptides as drug carriers. *Nucleic Acid and Peptide Aptamers edition of the Methods in Molecular Biology series*, Humana Press Inc., Totowa, USA, accepted.

(37) Kaplan, I. M., Wadia, J. S., and Dowdy, S. F. (2005) Cationic TAT peptide transduction domain enters cells by macropinocytosis. *J. Controlled Release 102*, 247–253.

(38) Duchardt, F., Fotin-Mleczek, M., Schwarz, H., Fischer, R., and Brock, R. (2007) A comprehensive model for the cellular uptake of cationic cell-penetrating peptides. *Traffic 8*, 848–866.

(39) Futaki, S., Nakase, I., Tadokoro, A., Takeuchi, T., and Jones, A. T. (2007) Arginine-rich peptides and their internalization mechanisms. *Biochem. Soc. Trans. 35*, 784–787.

(40) Singh, R. D., Puri, V., Valiyaveettil, J. T., Marks, D. L., Bittman, R., and Pagano, R. E. (2003) Selective caveolin-1-dependent endocytosis of glycosphingolipids. *Mol. Biol. Cell 14*, 3254–3265.

(41) Torgersen, M. L., Skretting, G., van Deurs, B., and Sandvig, K. (2001) Internalization of cholera toxin by different endocytic mechanisms. *J. Cell Sci. 114*, 3737–3747.

(42) Kirkham, M., Fujita, A., Chadda, R., Nixon, S. J., Kurzchalia, T. V., Sharma, D. K., Pagano, R. E., Hancock, J. F., Mayor, S., and Parton, R. G. (2005) Ultrastructural identification of uncoated caveolin-independent early endocytic vehicles. *J. Cell Biol. 168*, 465–476.

(43) Kirkham, M., and Parton, R. G. (2005) Clathrin-independent endocytosis: new insights into caveolae and non-caveolar lipid raft carriers. *Biochim. Biophys. Acta 1745*, 273–286.

(44) Harush-Frenkel, O., Debotton, N., Benita, S., and Altschuler, Y. (2007) Targeting of nanoparticles to the clathrin-mediated endocytic pathway. *Biochem. Biophys. Res. Commun. 353*, 26–32.

BC800172Q